Visualizing the water flow around a swimmer

Smedts, R.

Award date:
2012

Visualizing the water flow around a swimmer

Ruud Smedts (0718139)

November 2012

R-1814-S

Abstract

In this internship, we study the water motion around a swimmer using particle image velocimetry (PIV). We swim in the Tongelreep Innosport Lab, through a curtain of air bubbles. The disturbance of the bubbles is analysed using high speed underwater cameras. The films are then analysed using PIV. The techniques used and the problems encountered are discussed in the report.

The force generated by drag was found to be 48 N. This was for a swimmer who swam 1.5 m/s and whose hand was moving with 2.2 m/s backward. The force generated by lift is due to the vortices shed from the hand. We have tried to find these vortices using PIV. Vortex-like bubble motion could be seen. But a quantitative analysis turned out to be hard. The conclusion that can be drawn is that the order of magnitude of the lift force and the drag force are similar.

Contents

1 Introduction

At the InnoSportLab® in Eindhoven scientists develop systems and techniques to optimize the performance of top swimmers. One part of the work done there is doing measurements on swimmers. Examples are measuring the forces acting on a swimmer or the pressure distribution around the hand of a swimmer. Another part of the work done there is developing techniques to do measurements of the flow around on a swimmer.

At the moment a bubble system is installed in the pool. The goal of the system is to visualize the flow and especially the vortices around a swimmer and to use this to determine the forces acting on the swimmer. The path of the (rising) bubbles will be disturbed by the flow around a swimmer. The path is filmed by a high-resolution camera. The challenge is to develop software that can analyse these movies. In report essay the possibilities of different techniques to process the images will be examined.

The report is organised as follows. In the theory chapter some general information about particle image velocimetry and optical flow will be given. Further in this chapter one can read about the rise of bubbles in water, the thrust of an object in water and the forces acting on an object. Next an overview of the experimental set up will be given. After that the encountered problems will be discussed and the solutions used will be explained. In the end one can read the recommendations for further research.

2 Theoretical background

In this chapter we will first look into the theoretical possibilities for calculating the fluid dynamic forces from the velocity field. Then we explain what influences the rise speed of bubbles in water as we will use these in the experiments for visualising the flow. After that the ways of generating trust in water will be discussed and we will end with the techniques PIV and optical flow. These techniques can be used to get a velocity field from the images with bubbles.

2.1 Measuring fluid dynamic forces using the velocity field

The goal of the bubble system is not only to know the velocity field around a swimmer but also to know more about the forces acting on the swimmer. How the forces can be calculated from the velocity field will be explained in this paragraph.

In computational fluid dynamics the forces acting on a body are often calculated by direct evaluation of the pressure and shear stress on the surface on a body. But when PIV is used no information on the pressure field is known. Moreover, knowledge of the shear stress requires a very high resolution near the object boundary, which is very difficult using PIV. A method to calculate the forces using only the velocity and the vorticity field is explained by F. Noca (Noca, et al., 1997).

The evaluation starts with the well-known control-volume approach for momentum conservation:

$$\boldsymbol{F} = -\frac{d}{dt}\int_{V_m(t)} \rho \boldsymbol{u}\, dV + \oint_{S_m(t)} \boldsymbol{n}\cdot\boldsymbol{\Sigma}\, dS \qquad (1)$$

Here ρ is the fluid density, $\boldsymbol{u}$ is the velocity and $\boldsymbol{\Sigma}$ is the stress tensor which contains the pressure. The volume $V_m(t)$ is bounded on the inside by the body surface $S_b(t)$ and on the outside by surface $S_m(t)$ that is chosen at will with outward normal $\boldsymbol{n}$. The advantage of this force-balance description is that no flow information close to the body is needed, but it comes at the expense of having to evaluate a time-dependent term. Also, this formulation still needs the pressure field far away from the body, while the pressure field is hard to be come by experimentally. The pressure term can be eliminated. The proof can be found in (Noca, et al., 1999). The force for unit density is then, considering that the body is impenetrable, given by:

$$\begin{aligned}\boldsymbol{F} = -\frac{1}{N-1}\frac{d}{dt}\int_{V_m(t)} \boldsymbol{x}\times\boldsymbol{\omega}\, dV + \oint_{S_m(t)} \hat{\boldsymbol{n}}\cdot\gamma_{imp}\, dS \\ + \frac{1}{N-1}\frac{d}{dt}\oint_{S_b(t)} \boldsymbol{x}\times(\hat{\boldsymbol{n}}\times\boldsymbol{u})dS\end{aligned} \qquad (2)$$

Where

$$\gamma_{imp} = \tfrac{1}{2}u^2\mathbf{I} - \boldsymbol{u}\boldsymbol{u} + \tfrac{1}{N-1}\boldsymbol{\omega}(\boldsymbol{x}\times\boldsymbol{u}) + \tfrac{1}{N-1}\big(\boldsymbol{x}\cdot(\boldsymbol{\nabla}\cdot\mathbf{T})\big) + \mathbf{T},$$

$\boldsymbol{\omega}$ is the vorticity, N is the dimension, $\boldsymbol{u_s}$the velocity of the surface S_m(t), $\mathbf{I}$ is the unit tensor and $\mathbf{T}$ is the viscous stress tensor.

So as soon as the velocity field is known the forces can be calculated. The main advantages of using (2) instead of (1) are first of all that no information about the pressure is needed; second no gradients around the surface of the body have to be calculated. This is advantageous because the boundary layers can be very complex.

Although (2) has the desired property that no pressure is needed it still requires evaluation of the vorticity. It is interesting to investigate if (2) can be used to compute the forces due to isolated vorticity.

2.2 Rise speed of an air bubble in water

As air bubbles are used it is good to know more about the speed and forces acting on them. When air is released in water, air bubbles rise to the surface. The bubbles rise with a certain velocity which depends on the size and shape.

In general three regimes can be distinguished that show a different dependence on the bubble rise speed. The first regime is at very low *Re*, with very small spherical bubbles. The drag force here is dominated by viscosity and the rise speed increases with diameter. In the second regime, where the surface tension dominates, the bubbles are larger and no longer spherical. This is the regime with a Eötvös (*Eo*) number, $Eo = \Delta\rho g L^2/\sigma$, of $0.25 < Eo < 40$ (Clift, et al., 1978). Here σ is the surface tension and $\Delta\rho$ is the difference in density between the liquid and the bubble. In this regime the terminal velocity can increase, decrease or remain the same for different sizes. In the third regime *Eo* is high. The bubbles are then bullet shaped. And the forces are inertia dominated. The velocity increases for increasing bubble sizes.

2.2.1 Forces acting on a bubble

An air bubble released in water will rise to the surface. The terminal velocity of the bubble is determined by a force balance:

$$\boldsymbol{F}_g + \boldsymbol{F}_u + \boldsymbol{F}_d = \boldsymbol{0} \tag{3}$$

In which $\boldsymbol{F}_g$ is the gravitational force, $\boldsymbol{F}_u$ the upward force and $\boldsymbol{F}_d$ the drag force. The upward force is due to the buoyancy of the bubble. This is given by Archimedes' law:

$$\boldsymbol{F}_u = -V\rho_l \boldsymbol{g} \tag{4}$$

In which V is the volume of the bubble, ρ_l is the density of the water and $\boldsymbol{g}$ is the gravitational constant. In (4) it is assumed that the density of air is negligible. The gravitational force is $\boldsymbol{F}_g = m\boldsymbol{g}$, with m the mass of the bubble.

The magnitude of the drag force is given by (Batchelor, 1967):

$$F_d = \frac{\rho_l U^2 C_D A}{2} \tag{5}$$

Here U is the velocity of the bubble, C_D the drag coefficient and A is the cross section of the bubble. The most difficult variable to determine is the drag coefficient, as this one depends on the system's physiochemical properties and the bubble dimensions. (Kulkarni & Joshi, 2005).

2.2.2 Drag coefficient

The drag coefficient is a function of physiochemical properties of the system as well as the Reynolds number (*Re)*, $Re = UL/\nu$. In this L is the length of the object and ν is the kinematic viscosity of the liquid.

As these regimes differ a lot it was a challenge to find a general applicable correlation for the drag coefficient. A lot of researchers have worked on this problem and (Kulkarni & Joshi, 2005) give a review on this. Many correlations for the drag

coefficient in different regimes, for different contaminations etc. were found. But the most general applicable for single bubbles was formulated by (Rodrique, 2004):

$$C_D = \frac{\frac{16}{Re}\left(1 + 0.02Y^{\frac{10}{11}}\right)^{\frac{10}{11}}}{X^{\frac{21}{176}}} \tag{6}$$

$$X = (1 + 1.31 \cdot 10^{-5} \cdot Mo^{\frac{11}{20}} Y^{\frac{10}{11}})$$

$$Y = \left(\frac{3}{4} \cdot C_D Re^2 Mo\right)^{\frac{8}{9}}$$

$$Mo = \frac{g\mu^4 \Delta\rho}{\rho^2 \sigma^3}$$

Where μ is the dynamic viscosity. Although this looks complex and entirely empirical, there is a logical explanation for its general form. This can be appreciated as follows. First a dimensionless speed and acceleration are defined using the parameters of the problem;

$$V = \widetilde{U}U \text{ and } F = g\tilde{G} \tag{7}$$

$$\widetilde{U} = \left(\frac{\rho^2 d^2}{\sigma\mu}\right)^{\left(\frac{1}{3}\right)}, \tilde{G} = \left(\frac{\rho^5 d^8}{\sigma\mu^4}\right)^{\frac{1}{3}} \tag{8}$$

For a high Reynolds number it is known that drag coefficient is constant: $C_D = \frac{4gd}{3U^2}$. In the limit for the high Reynolds one can derive:

$$V \propto F^{\frac{7}{16}} \tag{9}$$

This can be checked as follows

$$V = \frac{U}{\widetilde{U}} \propto d^{\frac{7}{6}};\ F = \frac{g}{\tilde{G}} \propto d^{\frac{8}{3}} \rightarrow V \propto F^{\frac{7}{16}}$$

At low Reynolds numbers, the flow is laminar and the Hadamard-Rybczynski equation for laminar flow with slip is satisfied:

$$V = \frac{F}{12} \tag{10}$$

At intermediate Reynolds numbers it was found empirically that that

$$V = \frac{F}{12}\left(\frac{\left(1 + 1.31 \cdot 10^{-5} M^{\frac{11}{120}} F^{\frac{73}{33}}\right)^{\frac{21}{176}}}{\left(1 + 0.020 F^{\frac{10}{11}}\right)^{\frac{10}{11}}}\right) \tag{11}$$

In the limit for high velocities (11) is indeed proportional to $F^{\frac{7}{16}}$. And in the limit for low Reynolds it is indeed true that $V = \frac{F}{12}$.

As $F = \left(\frac{3}{4} C_D Re^2 M^{\frac{1}{8}}\right)^{\frac{8}{9}}$ formula (6) can be derived with elementary algebra.
For the bubbles used in the experiments the Reynolds number is about 10^2, the Morton number is in the order of 10^{-11}. This gives a drag coefficient of the order 1. With eq. (3) to (5) one can derive:

$$U = \sqrt{\frac{2gr}{3C_d}} \qquad (12)$$

With *r* the radius of the bubble. For the bubbles in with radii of about 0.5 cm the speed will be about 0.2 m/s.

2.3 Thrust in swimming

Propulsion in water can be achieved in two ways. The first method is thrust by drag, and the second is thrust by lift. Thrust by drag is the way a rowing boat propagates in the water. By pulling the oar backward a forward drag is the result. Because of this drag the rowing boat moves forward. When the oar is recovering to the start point, this is done above the water to have a minimal backward drag.

Thrust by lift is the way animals like whales propagate (figure 1). A whale flaps his tail and generates lift this way. The forward component of this lift makes the whale go forward. (Vogel, 1994)

Figure 1 Whales propagate by flapping their tails.

Both thrust by drag and thrust by lift have their own characteristics. Thrust by drag can only propel the boat as long as the oar water speed during the power stroke is positive. For example, during the power stroke the oar moves with 2 m/s. If the boat is stationary in the water the water speed of the oar is 2 m/s. When the boat moves at 1 m/s the water speed of the oar is just 1 m/s and less drag, thus thrust, is generated. As soon as the boat moves at 2 m/s the water speed of the oar is 0 m/s and no more thrust is generated (Vogel, 1994). Thus thrust by drag clearly has a maximum speed.

Thrust by lift also depends on the speed of the animal or the air foil. The greater the speed of the object relative to the water, the higher the lift is. But at higher speed also the backward drag increases. So the total thrust is a trade-off between backward drag and lift. A characteristic graph of the thrust versus the speed can be seen in figure 2.

One can conclude that in the low velocity regime more thrust can be generated by drag than by lift. Furthermore one can conclude that a higher maximum speed can be reached by lift than by drag.

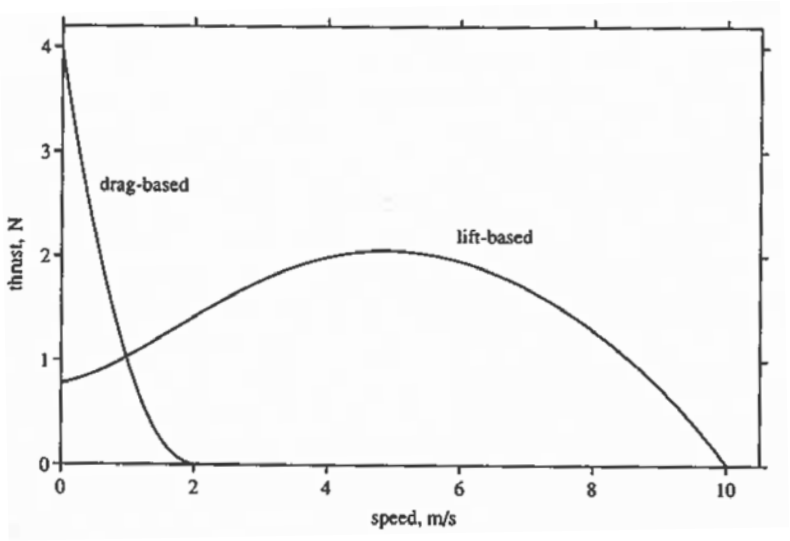

Figure 2 A typical curve relating thrust to speed for both drag-based and lift-based propulsion. (Vogel, 1994)

2.4 Drag coefficient of the human hand

A part of the thrust generated in swimming is due to drag at the swimmers hand. Therefore research has been done on the effect of spreading the fingers of a hand during swimming (Minetti, et al., 2009) and the angle of attack (Sato & Hino, 2003) on the drag coefficient.

It turned out that there is an optimal finger spacing and an optimal angle of attack. At the optimal finger spacing of 12° the drag coefficient is 8.8% greater than without spacing between the fingers. The angle of attack, as defined in figure 3, also has an effect on the drag coefficient. In (Sato & Hino, 2003) the drag and lift coefficients were calculated with a CFD model and compared to the experimental results. It turned out that the drag coefficient at the optimal angle of attack of 90° is about 1. For $50° < \alpha < 80°$ the drag coefficient is about 0.8.

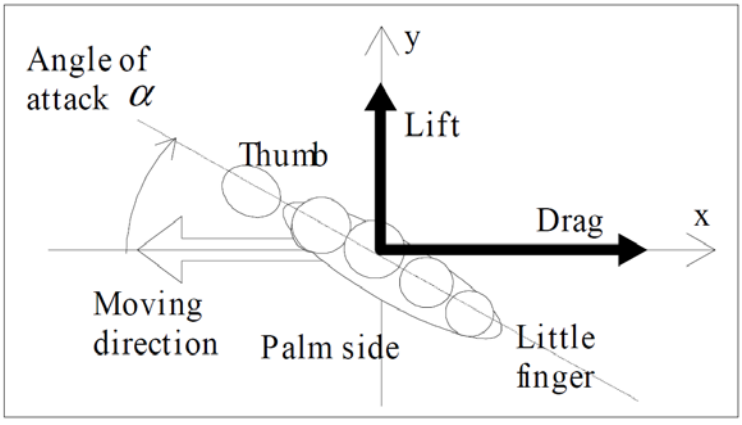

Figure 3 Definition of the angle of attack α and the drag and lift directions (Sato & Hino, 2003)

2.5 Particle image velocimetry

Particle image velocimetry (PIV) is a widely used technique in characterizing flow dynamics. There are many different ways of using PIV but the central concept is always the same. Namely, particles are placed in a fluid and the trajectories of these particles are captured in time. These trajectories indicate the flow. The number, size and type of particles differ for each method of PIV.

When only a small number of particles is used it is easy to follow a particle in time as the chance it overlaps with another particle is small. But if a large number of particles is used, cross correlation techniques have to be used to trace the patterns of particles (Adrian & Westerweel, 2011). The patterns will be traced by cross correlating parts of frames of a film. These parts are so called interrogation windows (figure 4).

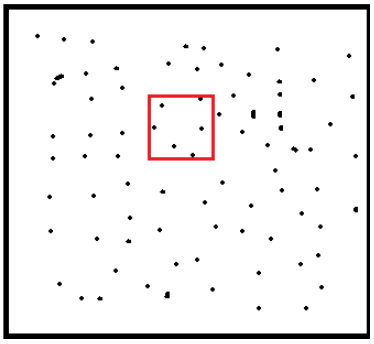

Figure 4 Interrogation window in a frame. The red box is the interrogation window, the black dots the particles and the black box the frame.

In the next frame the particles in the interrogation window will have moved. Some are still in the interrogation window. For these particles the displacement can be measured by crosscorrelating the two interrogation windows. Some particles will have moved out of the interrogation window, this is called ‘in plane losses’. Some particles have moved in a direction perpendicular to the plane and are therefore not in the interrogation window anymore, the ‘out of plane losses’. This result in a loss of information. A third kind of disturbance are the particles that are not in the interrogation window in the first frame but are in the second. So the only particles that help visualize the flow are particles that are both in the interrogation window in the first frame and in the second (figure 6, figure 5).

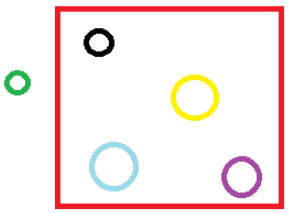

Figure 5 . Frame 1. The green particle is outside the interrogation window. The rest is inside.

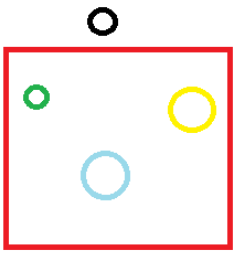

Figure 6. Frame 2, the black particle moved out the interrogation window. The green one moved in and the purple one moved in a tangential direction out of the plane.

2.5.1 Interrogation strategies

In the above paragraph the standard method of interrogation was presented. Here the interrogation window is the same size and on the same position in both the first and the second frame. The next interrogation window will then be placed next to the previous one or with a certain overlap. The overlap is to get more interrogation windows in the total frame and therefore reducing the number of in plane losses.

If more refined information about the flow is needed other techniques can be used, for example the so called multipass interrogation. In this technique the same image pair is interrogated multiple times using the same dimensions of the interrogation domain. The result of the first pass is then used to give the window an offset before running a second interrogation. This offset helps reducing the in plane losses. (Adrian & Westerweel, 2011). Then the second pass is used with the offset and therefore refining the results. More passes can be used if necessary.

A second way of getting more refined information is the multigrid interrogation (Adrian & Westerweel, 2011). The multigrid technique is similar to the multipass technique. The main difference is that in each subsequent pass the dimensions are reduced. The first pass has the biggest dimensions i.e. 64x64 pixels, the second pass then has the dimensions of 32x32 pixels etc. The advantage of the multigrid over the multipass approach is that the use of larger interrogation windows in previous passes ensures that the in plane losses are small.

As all these techniques are computational expensive the correlations parts of the images are often masked. This means that only the interesting parts of the flow are interrogated. This way only a part of the calculations is necessary.

2.6 Optical Flow

Another way of visualizing a movement in a picture is the so called optical flow. In this technique the assumption is made that intensities in a picture are conserved. This can of course only be true if the illumination is constant in time and the objects in the picture reflect light in the same way no matter where in the picture they are. But given the above assumption the conservation law can be written as (Jähne, 1991):

$$\frac{\partial g}{\partial t} + (\boldsymbol{f} \cdot \nabla) g = 0 \tag{13}$$

In this g is the intensity and $\boldsymbol{f(x,t)}$ is the velocity field in the picture. The goal is therefore to find $\boldsymbol{f}$.

Determining $\boldsymbol{f}$ is not trivial. One could try to find a minimum of the squared error of (13) with respect to variation of f_x and f_y:

$$e = < \left(\frac{f_x \partial g}{\partial x} + \frac{f_y \, \partial g}{\partial y} + \frac{\partial g}{\partial t} \right)^2 > \tag{14}$$

Where <..> is a local average. Minimizing e is done by calculating:

$$\begin{aligned} \frac{\partial e}{\partial f_x} &= < \frac{2 \partial g}{\partial x} \left(f_x \frac{\partial g}{\partial x} + f_y \frac{\partial g}{\partial y} + \frac{\partial g}{\partial t} \right) > = 0 \\ \frac{\partial e}{\partial f_y} &= < \frac{2 \partial g}{\partial y} \left(f_x \frac{\partial g}{\partial x} + f_y \frac{\partial g}{\partial y} + \frac{\partial g}{\partial t} \right) > = 0 \end{aligned} \tag{15}$$

Generally this is equation is very difficult to solve because of the gradient operators on an image.

2.6.1 Variational Approach

Another method to find $\boldsymbol{f}$ is to use a variational approach (Jähne, 1991). In this the error functional is written as follows:

$$\epsilon(f) = \int L(f, \nabla f, \boldsymbol{x}) d\boldsymbol{x} \tag{16}$$

Again a minimum for ϵ should be found. If the velocity field $\boldsymbol{f}$ is perturbed with a perturbation δ, which vanishes at the boundaries and $\boldsymbol{f}$ is one dimensional then the variation of ϵ is:

$$\epsilon(f + \delta) - \epsilon(f) = \int \left(\frac{\partial L}{\partial f} \delta + \frac{\partial L}{\partial f_x} \frac{d\delta}{dx} \right) dx \tag{17}$$

This is obtained by using a Taylor expansion. (17) can be rewritten by using integration by parts to:

$$\epsilon(f + \delta) - \epsilon(f) = \int \left(\frac{\partial L}{\partial f} - \frac{\partial}{\partial x} \left(\frac{\partial L}{\partial f_x} \right) \right) \delta dx \tag{18}$$

To make sure (18) goes to zero for an arbitrary δ, $\left(\frac{\partial L}{\partial f} - \frac{\partial}{\partial x} \left(\frac{\partial L}{\partial f_x} \right) \right) = 0$. In more dimensions this leads to:

$$\left(\frac{\partial L}{\partial f_i} - \frac{\partial}{\partial x_j}\left(\frac{\partial L}{\partial f_{x_j}}\right)\right) = 0 \tag{19}$$

This is the Euler-Lagrange equation. If the Lagrangian is taken to be:

$$L = \left((\boldsymbol{f} \cdot \nabla g) + \frac{\partial g}{\partial t}\right)^2 \tag{20}$$

Then

$$\frac{\partial L}{\partial f_i} = 2\left((\boldsymbol{f} \cdot \nabla) g + \frac{\partial g}{\partial t}\right)\frac{\partial g}{\partial x_i} \tag{21}$$

This is the same as (15) so little has been gained. Howerver, now the Lagrangian can be designed to include extra conditions the velocity field, such as requirements on smoothness. If the condition is that the field is smooth then the field has small spatial derivatives. Thus a suitable smoothness term requires spatial partial derivatives. A Lagrangian with suitable terms might be (Jähne, 1991):

$$L = \left(\nabla g\, \boldsymbol{f} + \frac{\partial g}{\partial t}\right)^2 + \alpha^2((\nabla f_1)^2 + (\nabla f_2)^2) \tag{22}$$

Here α is the smoothness factor and f_i is the i-th term of $\boldsymbol{f}$. With this Lagrangian the Euler-Lagrange equation becomes:

$$\left((\boldsymbol{f} \cdot \nabla) g + \frac{\partial g}{\partial t}\right)\frac{\partial g}{\partial x_i} - \alpha^2 \nabla^2 f_i = 0 \tag{23}$$

Starting from a trial field $\boldsymbol{f}(\boldsymbol{x})$ equation (23) can be solved as a diffusion equation,

$$\frac{\partial \boldsymbol{f}}{\partial t} = \alpha^2 \nabla^2 \boldsymbol{f} - \left(\boldsymbol{f} \cdot \nabla g + \frac{\partial g}{\partial t}\right)\nabla g \tag{24}$$

This is a monotonically decreasing function towards the stationary solution, the solution to the Euler Lagrange equation.

The regularization factor α^2 is a diffusion constant. By tuning the regularization constant to the velocity field that one wants to highlight it might be possible to see specific parts of the flow i.e. rotations. The gradient term is written as follows to illustrate this.

$$\begin{aligned} &|\nabla f_1|^2 + |\nabla f_2|^2 \\ &= \frac{1}{2}\left(\left(\frac{\partial f_1}{\partial x_1} + \frac{\partial f_2}{\partial x_2}\right)^2 + \left(\frac{\partial f_1}{\partial x_1} - \frac{\partial f_2}{\partial x_2}\right)^2\right. \\ &\left. + \left(\frac{\partial f_1}{\partial x_2} + \frac{\partial f_2}{\partial x_1}\right)^2 + \left(\frac{\partial f_1}{\partial x_2} - \frac{\partial f_2}{\partial x_1}\right)^2\right) \end{aligned} \tag{25}$$

The first term is the dilatation term which should be zero because $\nabla \cdot \boldsymbol{f} = 0$. The second and third term are the strain and the last term is the rotation term. If one is interested in the rotation then (25) should be smoothed with respect to the dilatation and the strain term.

In this case we omit the last term and (22)(4) becomes:

$$L^{\star} = \left(\frac{\partial f_1}{\partial x_1}\right)^2 + \left(\frac{\partial f_2}{\partial x_2}\right)^2 + \frac{1}{2}\left(\left(\frac{\partial f_1}{\partial x_2}\right)^2 + \left(\frac{\partial f_2}{\partial x_1}\right)^2\right) + \frac{\partial f_1}{\partial x_2}\frac{\partial f_2}{\partial x_1} \quad (26)$$

$$\frac{\partial}{\partial x_1}\frac{\partial L^{\star}}{\partial f_{x_j}} = 2\left(\frac{\partial^2 f_1}{\partial x_1^2} + \frac{\partial^2 f_1}{\partial x_1 \partial x_2} + \frac{\partial^2 f_2}{\partial x_2^2} + \frac{\partial f_2}{\partial x_1 \partial x_2}\right) \quad (27)$$

Furthermore the Euler-Lagrange equation becomes:

$$\left((\boldsymbol{f}\cdot\nabla)g + \frac{\partial g}{\partial t}\right)\frac{\partial g}{\partial x_i} - \alpha^2\left(\frac{\partial^2 f_1}{\partial x_1^2} + \frac{\partial^2 f_1}{\partial x_1 \partial x_2} + \frac{\partial^2 f_2}{\partial x_2^2} + \frac{\partial f_2}{\partial x_1 \partial x_2}\right) = 0 \quad (28)$$

Now (28) should be solved by writing it as a diffusion equation as has been done with (23).

Due to the limited time available for this project the usefulness of optical flow in analysing the data has not been tested. It is a good thing to try in new projects.

3 Experimental setup

In the InnoSportLab® a bubble system is installed on the bottom of a swimming pool. The system is about 1m wide and 8m long. It consists of one long tube with shorter tubes about 20cm separated attached to it. In the short tubes holes are made from which the bubbles are released (figure 7). The long tube is attached to a compressor which generates the compressed air. In the water an underwater camera is placed. The camera makes a movie at 50 Hz and of a resolution of 1920x1080 pixels. A typical frame from the movie can be seen in figure 8. In the figure the streams of bubbles coming from small tubes can and a swimmer be observed. The movies made with the camera are recorded on pc for further processing.

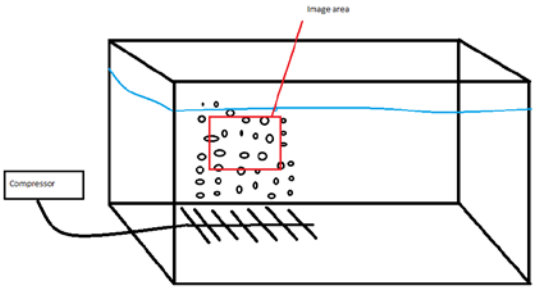

Figure 7 Schematic view of the bubble system

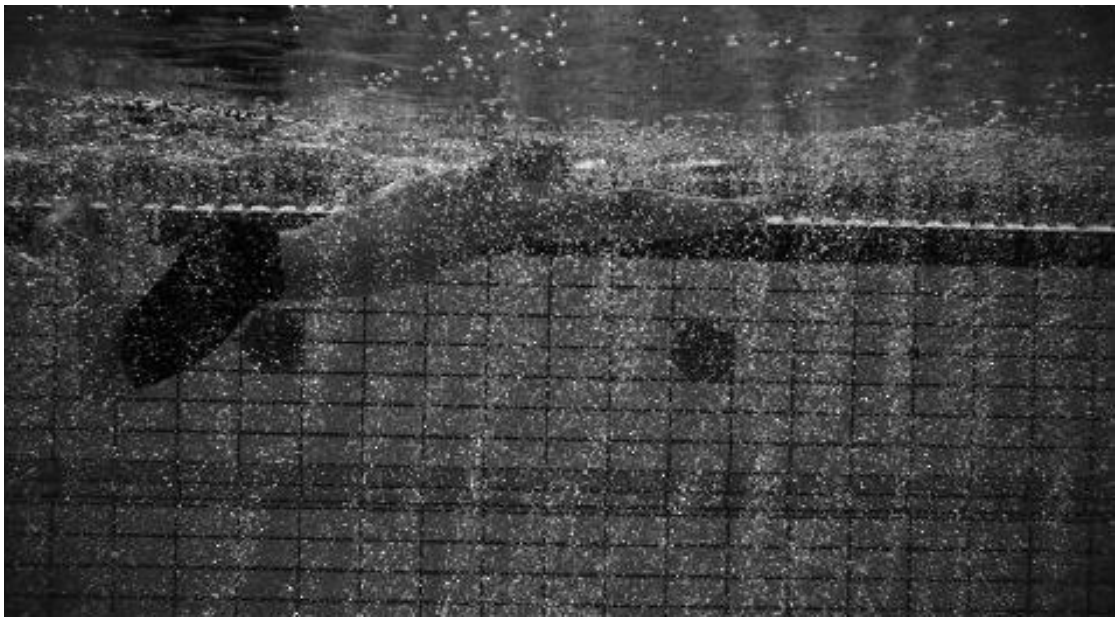

Figure 8 Example of a frame with swimmer

4 Results

A first attempt was made to use PIV on the recorded frames. In these frames a swimmer is observed performing butterfly kicks under water. For the leg strokes in butterfly kicks, thrust is generated principally by lift forces and the challenge was to observe the associated generation of vorticity. It will turn out that observation of these vertical events requires a better resolution than was provided in these movies. In addition problems arise when bubbles pass in front of the swimmer and when a background is visible in the images. In the next paragraphs these problems will be discussed. In paragraph 4.3 an experiment that copes with all these problems will be discussed and a quantitative analysis will be given on the forces acting on the swimmer.

4.1 Using MatPiv on recorded frames

A Matlab program called MatPiv was used directly on the frames. This program calculates the cross correlations of the consecutive interrogation windows and finds the peaks. For interrogation where no peaks could be found the velocity field is calculated by interpolating the adjacent interrogation windows. A region of interest was defined so the region without bubbles is excluded from the calculations. Furthermore MatPiv does four iterations, two times with interrogation windows of 64x64 pixels and two times with interrogation frames of 32x32 pixels. By doing multiple iterations the interrogation window can be adjusted to the field found in the previous iteration as explained in 2.5.1.

For frames without a swimmer the bubble rise is clearly visible in figure 9. The average rise speed of the bubbles is (26 ± 6) cm/sec. This is in line with the theory described in 2.2.2. When the program is used on a frame with swimmer still only the main field of rising bubbles can be seen in figure 10. This is because the bubbles that rise in front of the swimmer are more prominent than the bubbles disturbed by the swimmer. So this approach does not reveal the vortices of interest.

4.2 Filtering out the background

When using PIV the result one gets is an average displacement over the interrogation window. In case there is a non-uniform background this will disturb the results. In case of the swimming pool there are joints and tiles in the background. The average displacement is thus disturbed. This can be seen in figure 11. The wall of the swimming pool is visible. A way to get rid of these disturbances is filtering out the background.

The filtering can be done by averaging the movie over 100 frames. The result is shown in figure 12. The background without bubbles is clearly visible now. The background can then be subtracted from the frames. An example of how this works out is visible in figure 13. Now only the bubbles are visible in the picture. The contrast has been enhanced to make the bubbles more visible in a printed copy.

If PIV is used on these images it results in figure 14. It is clear that the background problem is solved this way as the background is no longer visible in the image. But still filtering out the background does not solve the problem of bubbles in front of the swimmer.

A way to emphasize disturbances in the PIV result is to subtract the average velocity field from the result. The average field is calculated over 100 frames in which no swimmer passes by. The result is visualized in figure 15. The outliers from the PIV routine are now more dominant. But no vortices are visible.

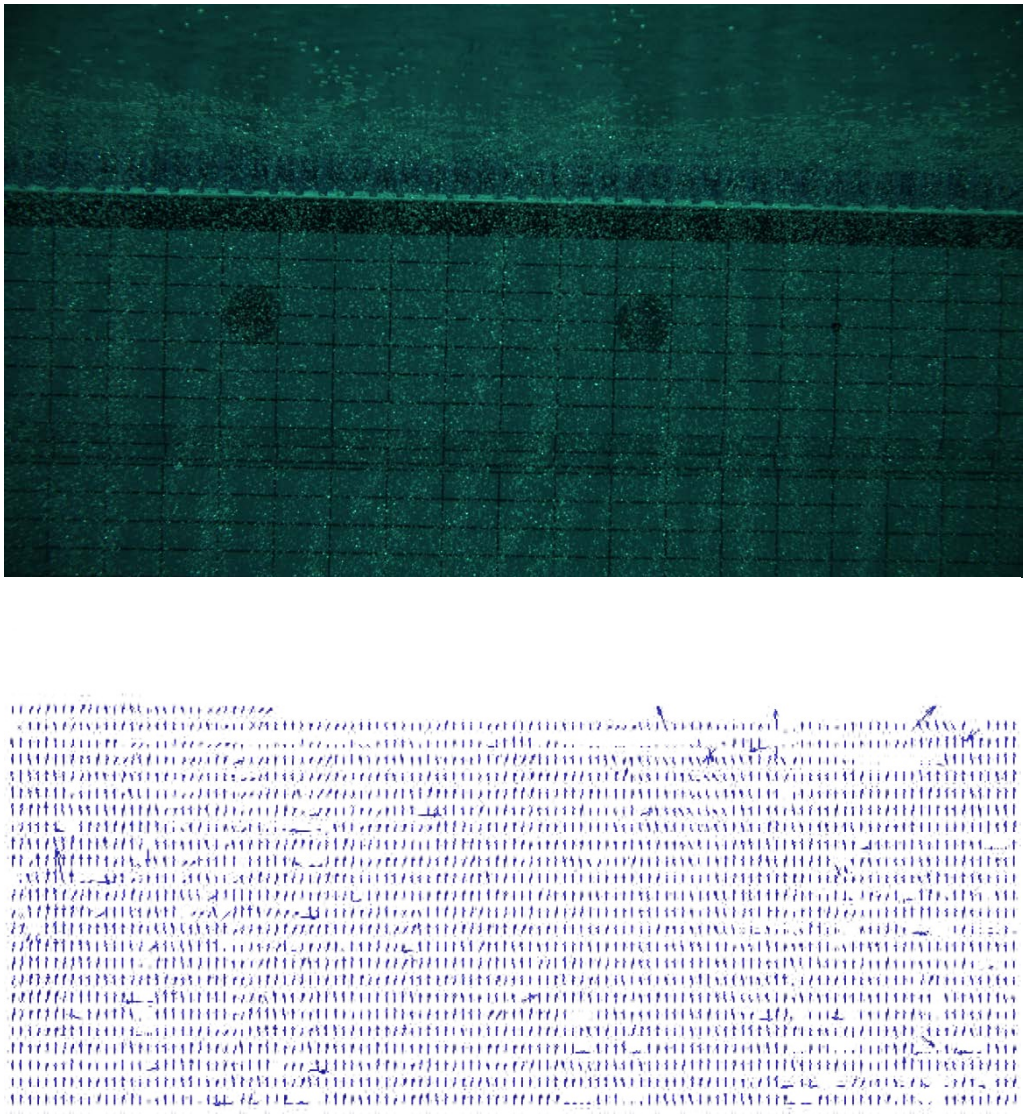

Figure 9 Picture of the rising bubbles and the corresponding vector field

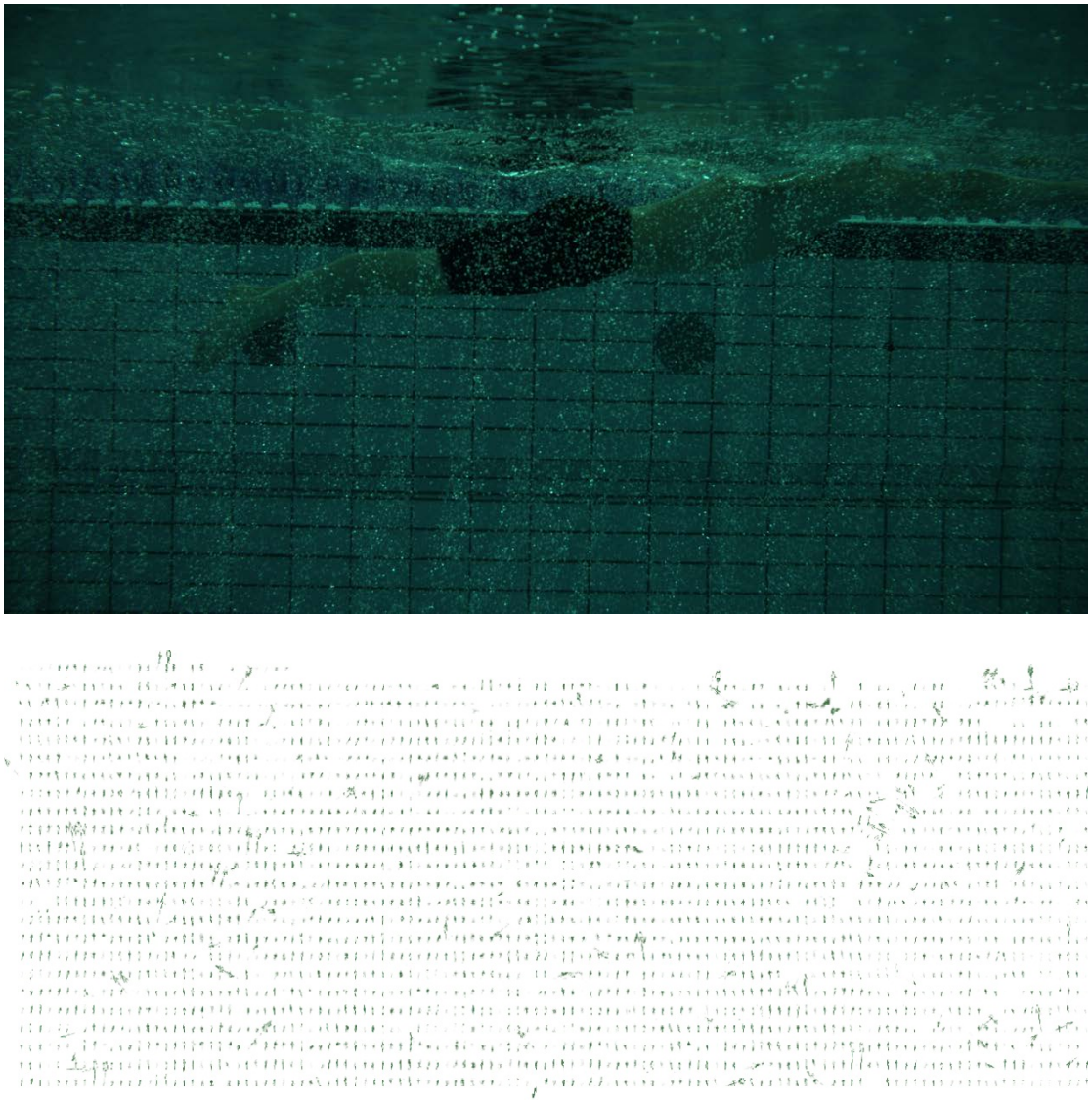

Figure 10 Frame with a swimmer and the corresponding vectorfield

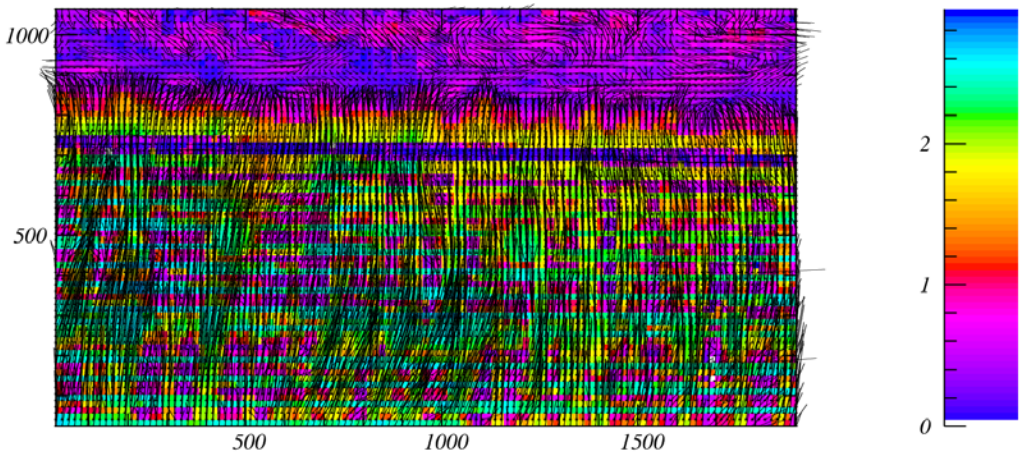

Figure 11 PIV results without filtering in the velocity field. The background of the pool is visible in the velocity field. Scale is in pixels.

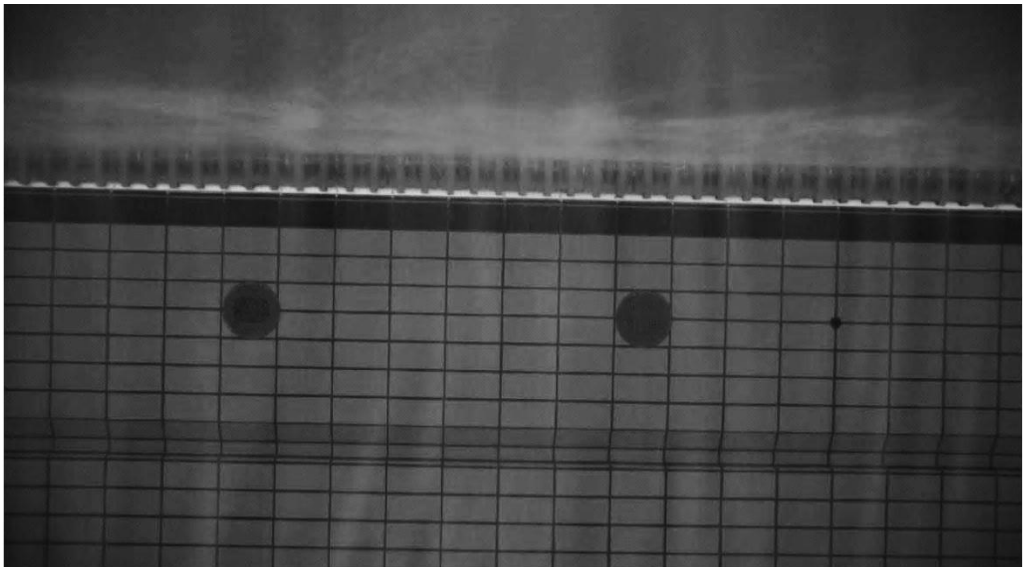

Figure 12 Background acquired by averaging over 100 frames.

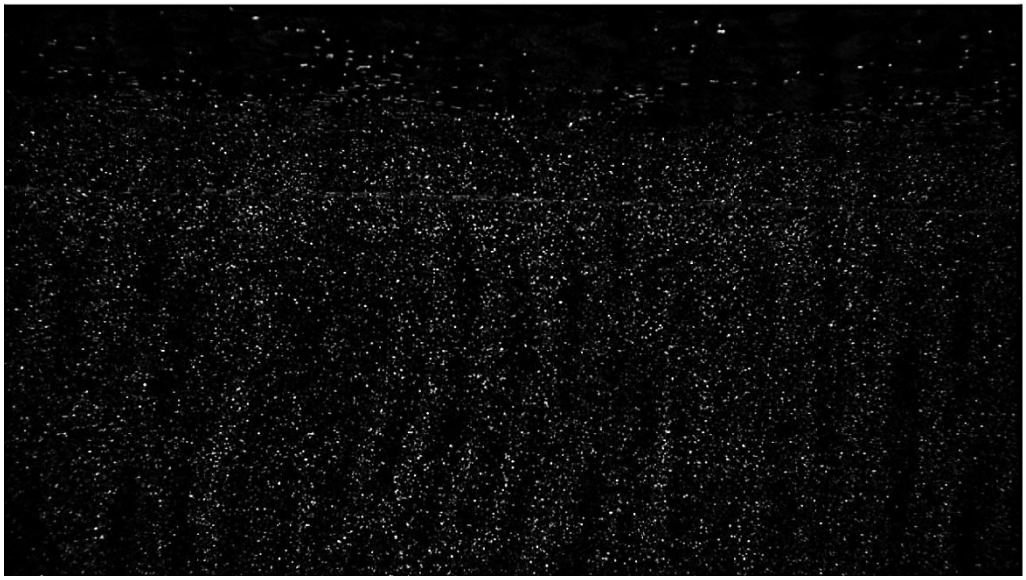

Figure 13 An example frame where the background is filtered out. The contrast has been enhanced to make the bubbles more visible.

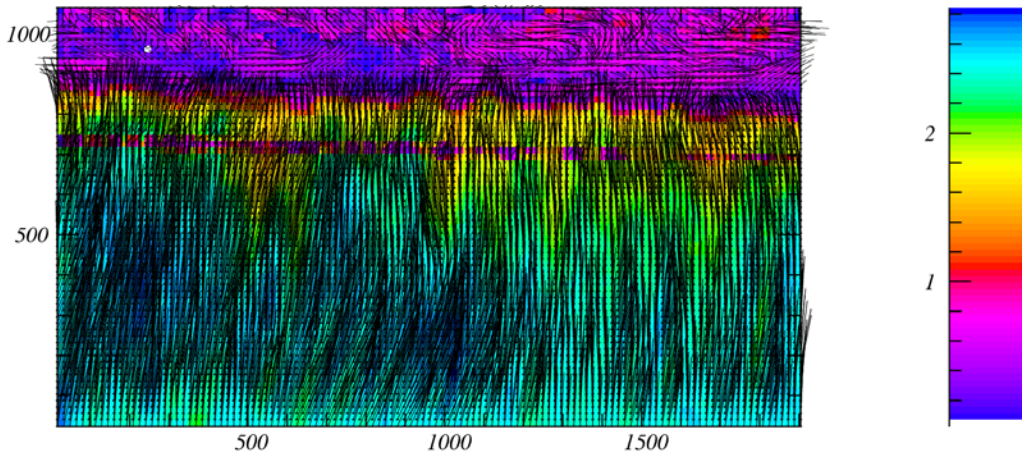

Figure 14 PIV results when the background is filtered out. The background is no longer visible. Scale is in pixels.

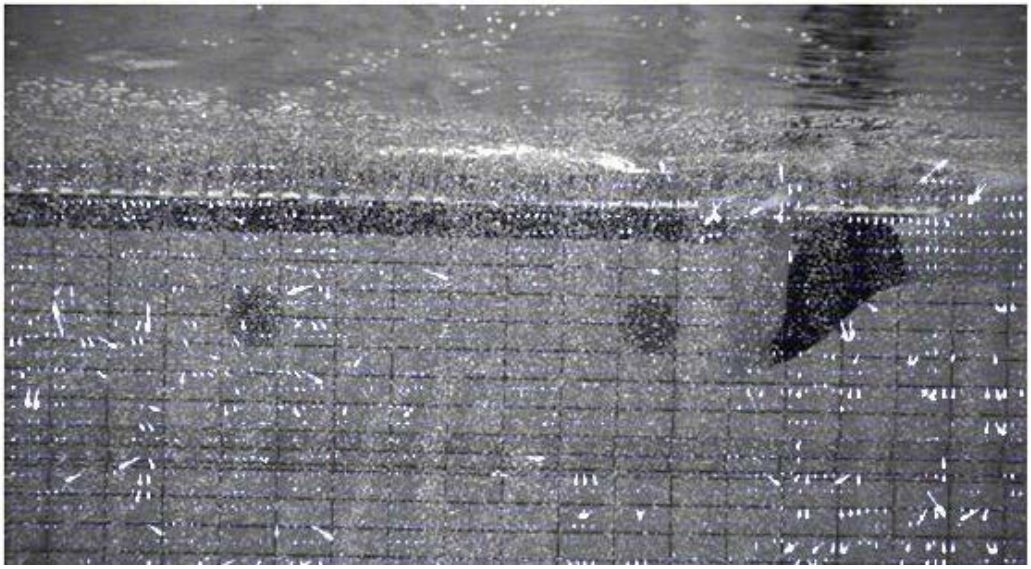

Figure 15 Average velocity field subtracted from the calculated field

4.3 Zooming in on details

The main problem with the above measurements is that the bubbles that rise in front of the swimmer are way more prominent than the disturbed bubbles. New images were made. In these images the swimmer is positioned not in the middle of the bubble system but at the edge closest to the camera. Therefore less bubbles rise in front of the swimmer. Besides this, special attention is paid to the bubbles around the hand of the swimmer.

A total of 100 frames have been correlated with their subsequent frame. The results of some of these correlations are shown in figure 16 to figure 17. It is possible to see disturbances of the bubbles in these images. A qualitative analysis is possible to be made with these results. This is a major improvement compared to the previous acquired images.

4.3.1 Forces and speeds involved

Multiple quantitative analyses can be performed on the images. One of the analyses is a check of the reliability of the PIV results. To do this the speed of the shoulder was found using PIV and by analysing the displacement in the images. It turned out that these were within 10% of each other.

Another thing analysed was the force generated by drag. For this the speed of the swimmer's hand relative to the water is needed. The speed of the swimmer turned out to be 1.5 m/s. The hand of the swimmer had a speed of -2.2 m/s at 90° relative to the surface. The surface of the hand is about $2.5 \cdot 10^{-2}\text{m}^2$. The drag coefficient is taken to be 0.80 as discussed in paragraph 2.4. The drag force generated by the hand at this point is then:

$F = \frac{1}{2} v^2 C_D A \rho = 48\text{N}.$

This is in agreement with the simulations done by (Sato & Hino, 2003).

For the lift force given by: $F_L = \rho v \Gamma L$, $\Gamma = \oint uds$, the circulation Γ needs to be found. According to the simulations done by (Sato & Hino, 2003) the lift coefficient is about half the drag coefficient, therefor we expect the lift force to be about half the

drag force. To determine the resolution that is needed to find a lift force of this order the width of the disturbances seen is measured. This was about 5 cm; this is about 4 interrogation windows (figure 18). If the lift force is indeed 25N the speed difference between the bubbles moving up and the bubbles moving down should be about 3m/s. The difference found was about 1 m/s. This is a very rough estimate as it is based on only 4 interrogation windows. For future measurements a higher resolution of the vortices is needed.

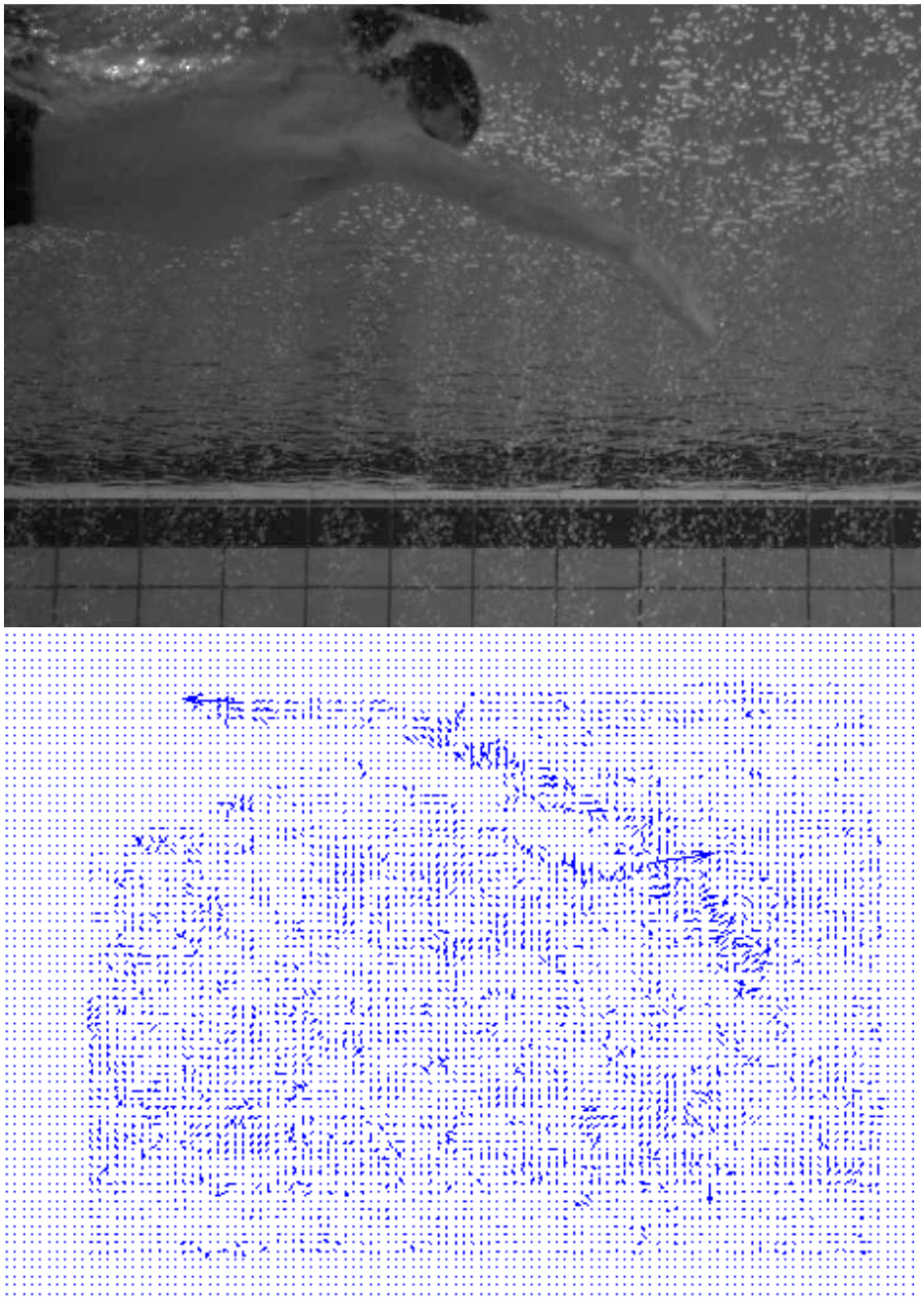

Figure 16 Disturbances around the arm are visible

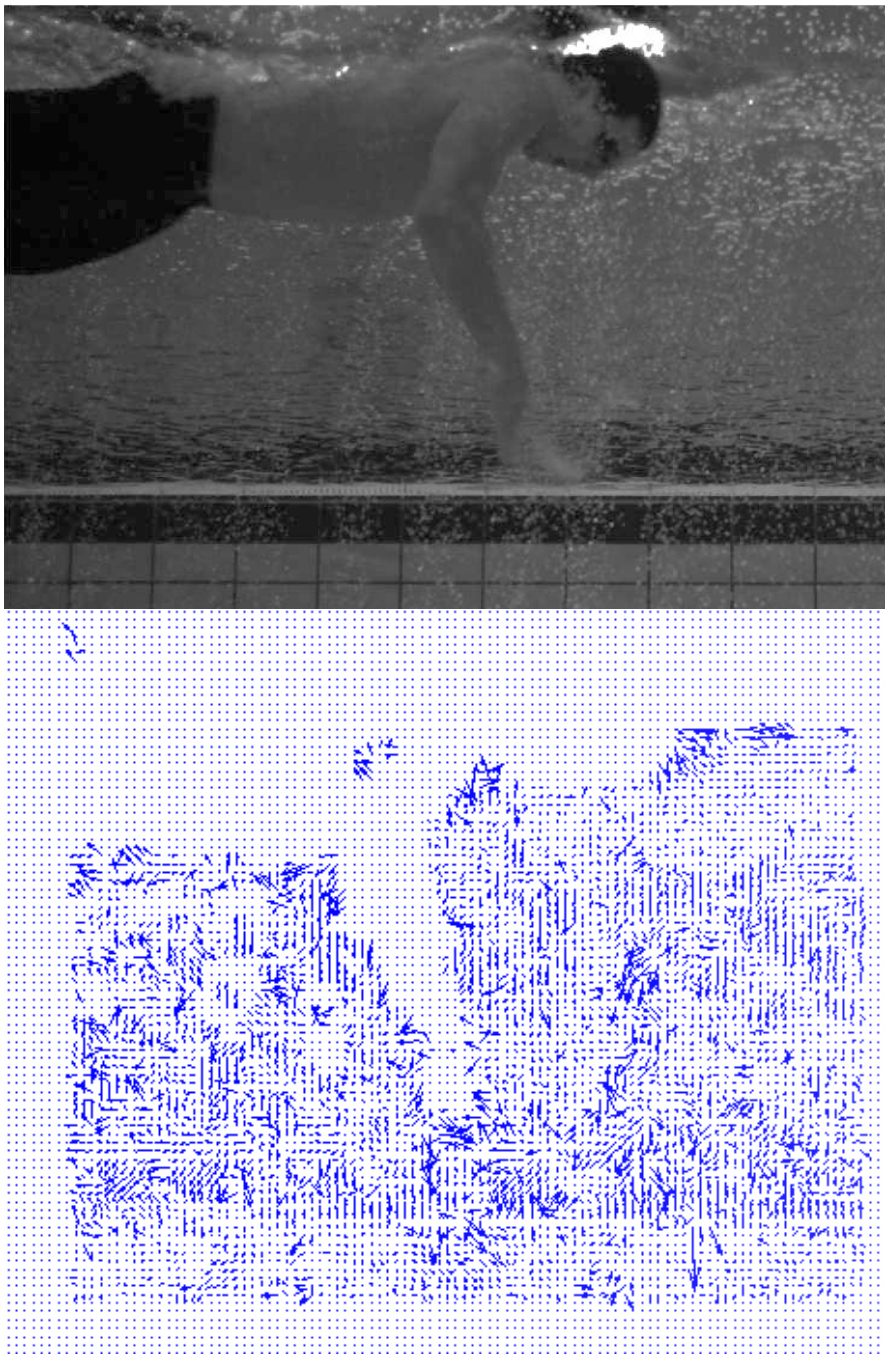

Figure 17 Disturbances in the water are visible

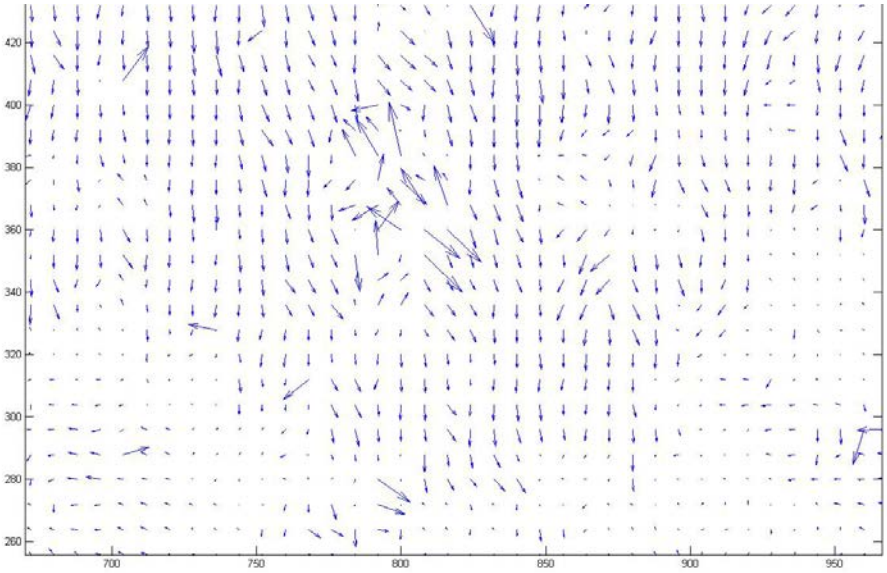

Figure 18 A vortex visible in the PIV results

5 Conclusions and recommendations

It turned out that by using particle image velocimetry it is possible to quantize the velocity of bubbles in water. To get good results a uniform and stationary background is needed.

The bubbles generated by the bubble system in the InnoSportLab in the Tongelreep could be used to visualize disturbances in the water made by a swimmer. Quantisation of these disturbances turned out to be hard because of an in stationary background and a too low resolution. From these disturbances it was possible to get the order of magnitude of the lift force generated by the hand of the swimmer. This was 10 N.

The drag force generated by the hand of the swimmer could be found from an estimate of the drag coefficient and the images from the high speed cameras. It turned out that the drag force was about 48 N.

For further the following recommendations can be made:

- Make sure the background is uniform for example by placing a screen behind the swimmer
- Make sure the background is stationary, so do not tilt the camera up too much as this makes the non-stationary water surface visible
- Adjust the bubble system so the bubble sheet is smaller and more uniform. This way more footage is useful.
- Zoom in on the disturbances to achieve a higher resolution

6 Bibliography

Adrian, R. J. & Westerweel, J., 2011. *Particle Image Velocimetry.* 1st ed. s.l.:Cambridge University Press.

Batchelor, G., 1967. An introduction to fluid dynamics. In: Cambridge: Cambridge University Press, p. 233.

Clift, R., Grace, J. R. & Weber, M. E., 1978. *Bubbles, Drops and Particles.* Londen: Academic Press.

Jähne, B., 1991. Digital Image Processing. In: Berlin: Springer-Verlag, pp. 297-317.

Kulkarni, A. A. & Joshi, J. B., 2005. Bubble Formation and Bubble Rise Velocity in Gas-Liquid Systems: A Review. *Industrial & Engineering Chemistry Research,* April, pp. 5918-5922.

Minetti, A. E., Machtsiras, G. & Masters, J. C., 2009. The optimum finger spacing in human swimming. *Journal of Biomechanics,* Volume 42, pp. 2188-2190.

Noca, F., D., S. & Jeon, D., 1997. Measuring instantaneous fluid dynamic forces on bodies, using only velocity fields and their derivatives. *Journal of Fluids and Structures,* Issue 11, pp. 345-350.

Noca, F., Shiels, D. & Jeon, D., 1999. A comparison of the methods for evaluating time-dependent fluid dynamic forces on bodies, using only velocity fields and their derivatives. *Journal of Fluids and Structures,* Issue 13, pp. 551-578.

Rodrique, D., 2004. A general correlation for the rise velocity of single gas bubbles. *The Canadian Journal of Chemical Engineering,* 82(2), pp. 382-836.

Sato, Y. & Hino, T., 2003. *Estimation of trhust of swimmer's hand using CFD.* s.l., s.n.

Vogel, S., 1994. Life in Moving Fluids. In: Baskerville: Princeton University Press, pp. 283-287.